Surface band characters of the Weyl semimetal candidate material MoTe$_2$ revealed by one-step angle-resolved photoemission theory

Ryota Ono [1], Alberto Marmodoro [2], Jakub Schusser [3,4], Yoshitaka Nakata,[1] Eike F. Schwier,[4,5] Jürgen Braun,[6] Hubert Ebert,[6] Ján Minár,[3] Kazuyuki Sakamoto [1,7,8,9] and Peter Krüger [1,7,*]

[1]*Graduate School of Science and Engineering, Chiba University, Chiba 263-8522, Japan*
[2]*FZU-Institute of Physics of the Czech Academy of Sciences, Cukrovarnicka 10, CZ-162 53 Prague, Czech Republic*
[3]*New Technologies–Research Center, University of West Bohemia, Univerzitni 8, 306 14 Plzeň, Czech Republic*
[4]*Experimentelle Physik VII, Universität Würzburg, Am Hubland, D-97074 Würzburg, Germany*
[5]*Hiroshima Synchrotron Radiation Center, Hiroshima University, Kagamiyama 2-313, Higashi-Hiroshima 739-0046, Japan*
[6]*Department of Chemistry, Ludwig Maximilians University München, Butenandtstraße 11, 81377 Munich, Germany*
[7]*Molecular Chirality Research Center, Chiba University, Chiba 263-8522, Japan*
[8]*Department of Applied Physics, Osaka University, Osaka 565-0871, Japan*
[9]*Center for Spintronics Research Network, Graduate School of Engineering Science, Osaka University, Osaka 560-8531, Japan*

The layered two-dimensional material MoTe$_2$ in the T_d crystal phase is a semimetal which has theoretically been predicted to possess topologically nontrivial bands corresponding to Weyl fermions. Clear experimental evidence by angle-resolved photoemission spectroscopy (ARPES) is, however, lacking, which calls for a careful examination of the relation between ground state band structure calculations and ARPES intensity plots. Here we report a study of the near-Fermi-energy band structure of MoTe$_2(T_d)$ by means of ARPES measurements, density functional theory, and one-step-model ARPES calculations. Good agreement between theory and experiment is obtained. We analyze the orbital character of the surface bands and its relation to the ARPES polarization dependence. We find that light polarization has a major effect on which bands can be observed by ARPES. For s-polarized light, the ARPES intensity is dominated by subsurface Mo d orbitals, while p-polarized light reveals the bands mainly derived from Te p orbitals. Suitable light polarization for observing either an electron or hole pocket are determined.

I. INTRODUCTION

Topological Weyl semimetals (WSMs) are receiving much attention because the quasiparticles at particular points in the band structure are a realization of massless Dirac fermions, so-called Weyl fermions [1]. WSMs have peculiar transport properties [2–5], including the quantum anomalous Hall effect and the violation of separate number conservation laws for the left-handed and right-handed Weyl fermions in the presence of parallel electric and magnetic fields, known as the chiral anomaly [6]. In a semimetal, both the conduction and valence bands cross the Fermi energy. In a WSM, there are special crossing points, called Weyl points, which correspond to topologically protected states. Weyl points come in pairs with opposite chirality. They are the end points of the Fermi arc, i.e., the open Fermi line of the surface band structure. TaAs and related compounds were the first materials in which the WSM property was experimentally observed [1,7–9]. More recently, another possible realization of WSMs was found in transition metal dichalcogenides (TMDCs), e.g., WTe$_2$ [10–13]. TMDCs are two-dimensional (2D) layered materials and particularly promising for electronic applications. TaAs and WTe$_2$ are classified as type-I and type-II

WSMs, respectively [10]. Both types have pointlike crossings at the Fermi energy, but in the type-II WSM the cone-shaped bands are tilted in k space. Also, the type-I WSM respects Lorentz invariance, whereas type II breaks it [10].

The TDMC molybdenum tellurite, in the low-temperature MoTe$_2(T_d)$ phase, has been proposed as a possible WSM material [14–17]. At room temperature, MoTe$_2$ crystallizes in the monoclinic, centrosymmetric $1T'$ phase. Upon cooling below 240 K MoTe$_2$ changes to the orthorhombic, noncentrosymmetric T_d phase (space group $Pmn2_1$, No. 31) [18–21]. While the atomic structures of the $1T'$ and T_d phases are similar, the fact that the T_d phase lacks inversion symmetry makes it a possible realization of a type-II WSM, as proposed on both theoretical and experimental grounds [10,14–17]. The surface band structure of MoTe$_2(T_d)$ has been studied using angle-resolved photoemission spectroscopy (ARPES) by several authors [15–17,22], but the interpretation of the data is difficult without dedicated ARPES simulations including final state and matrix element effects. ARPES peak positions are routinely used for band mapping, but the peak intensities, which contain useful information about the electronic wave functions [23], are often left unexploited. The ARPES intensity and its light polarization dependence are determined not only by the initial state band character but also by final state effects, particularly in spin-orbit coupled systems [24] such as WSMs. As a consequence, reliable ARPES calculations

*pkruger@chiba-u.jp

within the one-step model of photoemission are necessary for a correct interpretation of the experimental data. To the best of our knowledge, such calculations have not been reported yet. Aryal and Manousakis investigated the ARPES intensity using the plane-wave approximation [25], which has many known shortcomings [26], especially for heavy elements like Mo and Te, where distorted wave effects are large.

Most ARPES studies of $MoTe_2(T_d)$ have focused on the search for topologically nontrivial Weyl points and Fermi arcs [14–17,22]. While density functional theory (DFT) calculations have consistently found these features in the $MoTe_2$ surface band structure, the experimental evidence remains elusive and controversial. This calls for a careful examination of the relation between the band dispersion predicted by ground state DFT and the ARPES intensity maps that are recorded in experiment. Moreover, the polarization dependence of ARPES can be utilized for highlighting different bands and for revealing their elemental and orbital character. The orbital character of the surface bands is important for technological applications since it determines the sensitivity of the electronic structure of the system against controlled and uncontrolled chemical reactions at the surface.

Here we report a detailed study of the surface band structure of $MoTe_2(T_d)$ by means of DFT calculations. We present ARPES calculations for this system using a one-step model description. We analyze the orbital character of the near-Fermi-level bands and predict a strong polarization dependence of the ARPES spectra. The calculated ARPES intensity maps are in good agreement with new, high-resolution experimental data obtained with a laser source. The results show how specific bands, and atomic species can be highlighted in ARPES with appropriate polarization, providing valuable guidelines for future ARPES measurements.

The rest of the paper is organized as follows. In Sec. II the computational and experimental methods are outlined. In Sec. III, the results of the ground state band structure and of the ARPES calculations are presented. The polarization dependence of the ARPES spectra is studied in detail and analyzed in terms of the orbital character of the bands. Then, the theoretical ARPES maps are compared with experiment. Finally, in Sec. IV we summarize and conclude our work.

II. THEORETICAL AND EXPERIMENTAL METHODS

Two types of calculations are performed. First, the ground state band structure at the $MoTe_2(T_d)$ surface is computed with DFT in a repeated slab geometry. Second, ARPES simulations are performed using the one-step model of photoemission. Throughout this paper, the experimental structure with lattice constants $a = 3.477$ Å, $b = 6.335$ Å, $c = 13.883$ Å [21] is used. The crystal structure is shown in Fig. 1. Surface relaxation has been checked with DFT and found to be negligible, as expected for layered materials with weak van der Waals forces between layers such as $MoTe_2$.

A. Ground state band structure calculations

The surface is modeled using a slab of four $MoTe_2$ layers and over 10-Å vacuum spacing between slabs, resulting in a supercell lattice parameter $c = 37.8$ Å. The
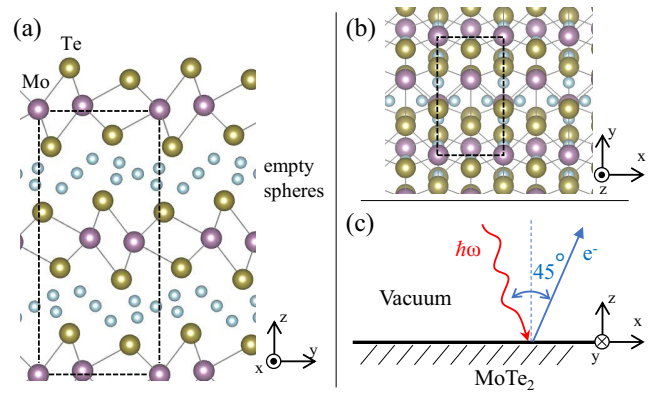

FIG. 1. (a) and (b) Ball and stick model of the $MoTe_2$ surface. Dashed lines indicate the unit cell. Mo is in purple, Te is in yellow, and empty spheres are in light blue. (a) Side view. (b) Top view. (c) Experimental geometry.

projector augmented-wave method as implemented in the Vienna Ab initio simulation package (VASP) [27] is used with the commonly adopted [14] Perdew-Burke-Ernzerhof (PBE) exchange-correlation functional [28]. The calculations are performed on a $16 \times 10 \times 1$ **k**-point mesh in the Brillouin zone, and the plane-wave basis energy cutoff is set to 400 eV. The spin-orbit interaction (SOI) is taken into account in all calculations.

B. One-step ARPES calculations

The ARPES calculations are done with the spin-polarized relativistic Korringa-Kohn-Rostoker (SPR-KKR) package [29]. As in the slab calculations, the experimental crystal structure and the PBE exchange-correlation potential are used. The SOI is treated exactly through the Dirac equation. The atomic sphere approximation (ASA) is used, and the KKR equations are solved with an angular momentum cutoff of $l_{max} = 3$. After computing the bulk Green's function, a surface model is constructed, and the Green's function of the semi-infinite surface is found by solving a Dyson equation. We perform one-step model ARPES calculations [29–32] for the semi-infinite surface model using the layered Korringa-Kohn-Rostoker (LKKR) multiple scattering theory [32–35].

As the crystal structure of $MoTe_2$ is not densely packed but contains a large interstitial volume, empty spheres must be added when using the ASA to obtain converged, self-consistent potentials. As a result, SPR-KKR yields a ground state band structure in excellent agreement with the VASP calculations. However, we found that the empty spheres inside $MoTe_2$ layers lead to numerical difficulties in the LKKR calculations needed for ARPES. The reason is related to the fact that in LKKR, compact 2D scattering layers must be defined. In $MoTe_2$ the crystal planes are rumpled, which may lead to complications when solving the multiple-scattering equations between layers [34,35]. Therefore, in the ARPES calculations, we have removed the empty spheres inside the $MoTe_2$ layers and kept only those between the layers [see Fig. 1(a)]. The same strategy has already been applied successfully to another TMDC material (WTe$_2$ [13,36]). As a result, the ARPES band
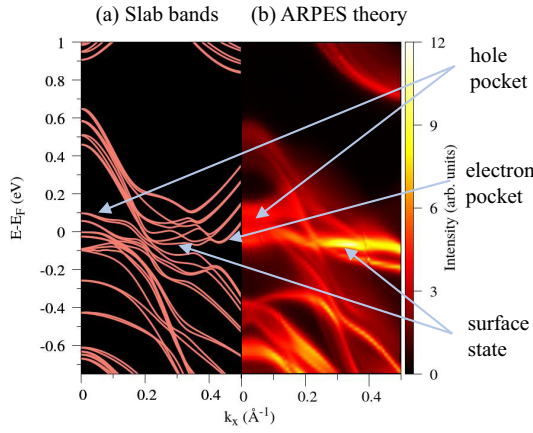
FIG. 2. Theoretical $MoTe_2$ band structure along $\overline{\Gamma}$-$\overline{X}$ of the 2D Brillouin zone. (a) Ground state slab model calculations. (b) ARPES calculations for unpolarized light and a photon energy of 60 eV.

dispersions of $MoTe_2$ agree well with the DFT-VASP bands, as seen in Fig. 2.

C. Experimental details

The $MoTe_2$ sample was grown by the chemical vapor transport method. After preparation at room temperature, the crystal was in the $1T'$ phase. During the ARPES measurements, however, the sample was in the T_d phase since it was maintained at a temperature of 67 K, which is well below the Td transition temperature (240 K). High-resolution ARPES measurements were performed at the μ-ARPES system of the Hiroshima Synchrotron Radiation Center (HiSOR), Japan [37]. Photoelectrons, which were excited by a vacuum-ultraviolet laser ($\hbar\omega = 6.27$ eV), were collected by a hemispherical photoelectron analyzer (VG Scienta R4000). The light was incident in the xz plane, making an angle of $45°$ with the electron emission direction [Fig. 1(c)]. The energy and spatial resolutions were better than 3 meV and 5 μm, and the angular resolution was better than $0.05°$.

III. RESULTS AND DISCUSSION

A. Band structure of $MoTe_2(T_d)$

In $MoTe_2(T_d)$, topologically nontrivial bands have been predicted near the $\overline{\Gamma}$-$\overline{X}$ line ($k_y = 0$) of the Brillouin zone between the hole pocket centered at $k_x = 0$ and the electron pocket around $k_x = 0.3$ Å^{-1} [14]. Here we focus on this region in $(\mathbf{k}, E)$ space. The DFT band structure obtained with the slab model is shown in Fig. 2 along with ARPES simulations for unpolarized light, obtained by summing over x-, y-, and z-linear polarization. Here we have chosen a photon energy of 60 eV as used in the experiments of Ref. [17]. The band dispersion in the ARPES map agrees well with the VASP-DFT band structure, which shows that the ASA used in the KKR calculations provides an accurate representation of the crystal potential of $MoTe_2$. The band structure in Fig. 2 is in good agreement with other calculations [14] and features an electron and a hole pocket along k_x, as well as a flat surface state.

B. Orbital-projected bands and ARPES polarization dependence

Here we analyze the orbital character of the bands near the Fermi level and the relation to the ARPES polarization dependence. In the one-step ARPES calculations, final state and matrix element effects are fully taken into account [31], and the predicted polarization dependence should be a reliable guide for experiments. In addition, a semiquantitative model of the polarization dependence based on the valence band structure alone is very useful and can be gained by considering optical selection rules. The $MoTe_2$ valence band near E_F is dominated by Mo $4d$ and Te $5p$ orbitals, as seen in Fig. S1 in the Supplemental Material [38]. We limit our analysis to these two orbitals. The photoemission intensity is proportional to the square of the transition matrix element

$$M_{if} = \langle \phi_f | \hat{\epsilon} \cdot \mathbf{r} | \phi_i \rangle, \tag{1}$$

where $|\phi_i\rangle$, $|\phi_f\rangle$, $\hat{\epsilon}$, and $\mathbf{r}$ are initial and final state wave functions, the light polarization vector, and the electron position operator, respectively. According to the dipole selection rules, an electron can transit from an initial state with angular momentum l to a final state of angular momentum $l \pm 1$. In the following, we discuss only $l \rightarrow l - 1$ transitions for simplicity. The $l \rightarrow l + 1$ transitions, which often dominate at high energy, give rise to a more complex, but generally less pronounced, polarization dependence. To see this, consider, e.g., a p_z initial state. The $l \rightarrow l - 1$ transition leads to an s-wave final state and a strong $\cos^2\theta$ polarization dependence, where θ is the angle between the electric field vector and the z axis. In particular, the intensity is zero for x- and y-linearly polarized light. In contrast, $l \rightarrow l + 1$ transitions from p_z to one of the five d orbitals are possible for any light polarization such that the intensity never vanishes.

In the $l \rightarrow l - 1$ channel considered here, only the following transitions are possible from Mo d and Te p initial states for linear polarized light: for x polarization, Te $p_x \rightarrow s$ and Mo $d_{xz} \rightarrow p_z$; for y polarization, Te $p_y \rightarrow s$, Mo $d_{yz} \rightarrow p_z$, and Mo $d_{xy} \rightarrow p_x$; and for z polarization, Te $p_z \rightarrow s$ and Mo $d_{z^2} \rightarrow p_z$. Other transitions are forbidden by the dipole selection rules. From these considerations, we expect that ARPES with x-polarized light will reveal the bands with a large Te p_x and Mo d_{xy} orbital character. The calculated ARPES spectra for 60-eV light and x polarization are compared with the DFT bands projected onto Te p_x and Mo d_{xz} orbitals in Fig. 3. Here and in all following DFT band plots, projection is done on the surface Te atoms and the subsurface Mo atoms. The Mo intensity is divided by a factor of 2 in order to roughly account for the ARPES surface sensitivity. Note that this Mo:Te weight ratio also corresponds to bulk $MoTe_2$. Most ARPES features can be well identified with either of the two initial states. DFT bands projected on other Te or Mo orbitals resemble the ARPES map much less, as can be seen in Figs. S2 and S3 in the Supplemental Material [38]. This indicates that the orbital character of the bands together with the $l \rightarrow l - 1$ dipole selection rules provides a qualitative understanding of the polarization dependence of the ARPES spectra. In Figs. 3(b) and 3(c), the strongest intensity appears around $k_x = 0$ Å^{-1} ($= \overline{\Gamma}$ in the 2D Brillouin zone) for both the Te p_x and Mo d_{xz} initial states. The ARPES for x polarization
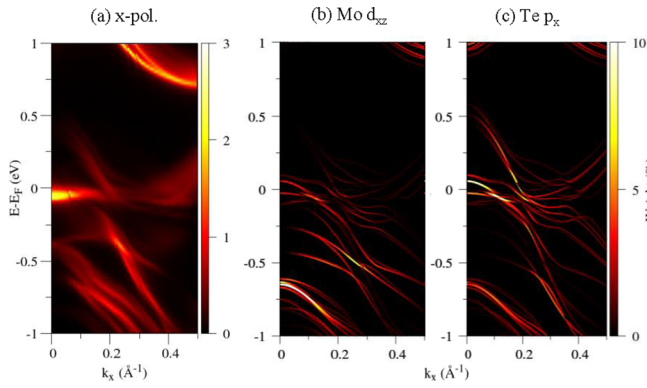
FIG. 3. (a) Calculated ARPES map for *x*-polarized light ($\hbar\omega = 60$ eV). Note the strong intensity at the hole pocket. DFT bands projected on (b) the Mo d_{xz} and (c) Te p_x orbitals.

FIG. 5. (a) Calculated ARPES intensity for *z*-polarized light ($\hbar\omega = 60$ eV). Note that the color scale is enhanced by a factor of 4 compared to Figs. 3 and 4. DFT bands projected on (b) the Mo d_{z^2} and (c) Te p_z orbitals.

is most intense around $k_x = 0$ Å^{-1} just below the Fermi level, which can be attributed to the Te p_x orbital. In addition, other high-intensity ARPES bands correspond to the hole pocket. As seen from Fig. 3 they are mainly due to Mo d_{xz} character. Small energy shifts exist between the KKR-computed ARPES bands and the VASP-DFT bands. This is expected because of the different approximations used in the two approaches, most importantly the atomic sphere approximation in KKR. With this in mind, the most intense Mo d_{xz} bands (at $E \sim -0.7$ eV, $k_x \sim 0$) also agree well with the ARPES bands. From the foregoing analysis, we conclude that linear polarization along the *x* axis is a good choice for observing the hole pocket in MoTe$_2$. In experiment, this corresponds to *s* polarization with light incidence in the *yz* plane.

The calculated ARPES spectra for *y* polarization and the corresponding projected bands are shown in Fig. 4. In the case of *y* polarization, $l \rightarrow l-1$ transitions are possible only from Mo d_{xy}, Mo d_{yz}, and Te p_y initial states. In the Mo d_{xy} and Mo d_{yz} projection, the dominant feature is a group of bands which disperses linearly from $k_x = 0$ Å^{-1}, $E = 0.5$ eV to $k_x = 0.4$ Å^{-1}, $E = -1$ eV. Closer inspection shows that they are made of two groups of bands, where the upper part

joins the electron pocket at $k_x \approx 0.3$ Å^{-1}. The lower part evolves into the hole pocket around the $\bar{\Gamma}$ point. These linearly dispersing bands are clearly seen as a bright feature in the calculated ARPES spectra. The projection on the Te p_z bands shows moderately intense bands in the region $k_x < 0.3$ Å^{-1}, $E < -0.7$ eV, which can explain the corresponding bands seen in the ARPES plot. However, the Te p_y contribution is very weak for all bands above -0.4 eV, and so the Te p_y orbital plays no role for the electron and hole pockets.

For both *x*- and *y*-polarized light, the calculated ARPES intensity is very weak compared to *z* polarization (see Fig. 5). This is because the considered *k* range around the $\bar{\Gamma}$ point of the Brillouin zone corresponds to near-normal emission, i.e., an emission direction perpendicular to the photon electric field vector in the *xy* plane. It is well known that perpendicular emission is generally much weaker than parallel emission [39]. In the popular plane-wave approximation, perpendicular emission is even impossible [23]. Yet the existence of some pronounced ARPES features at $\boldsymbol{k} = 0$ for both *x*- and *y*-polarized light shows that the plane-wave approximation can be misleading [26,40] and that one-step model
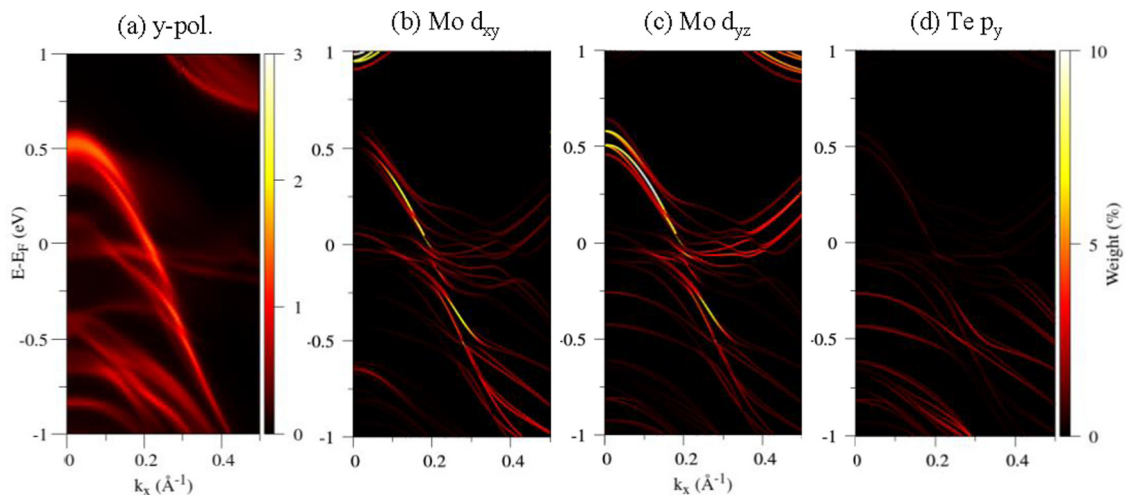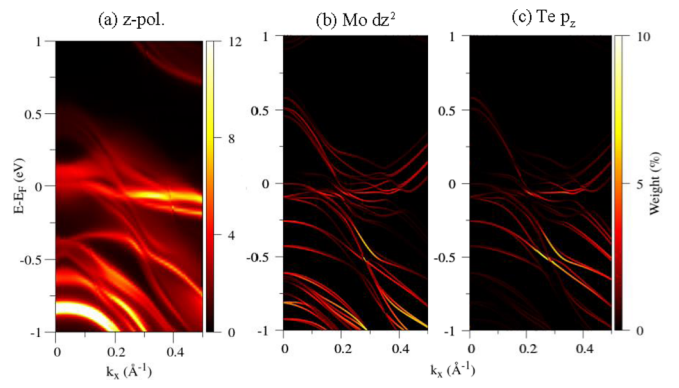

FIG. 4. (a) Calculated ARPES intensity for *y*-polarized light ($\hbar\omega = 60$ eV). A group of strong ARPES bands forms a linearly dispersing line. DFT bands projected on (b) the Mo d_{xy}, (c) Mo d_{yz}, and (d) Te p_y orbitals.

calculations are needed for a correct interpretation of ARPES spectra.

In Fig. 5 the calculated ARPES spectra for z polarization are shown along with possible orbital-projected DFT bands, namely, Mo d_{z^2} and Te p_z. The Mo d_{z^2} projection shows strong intensity for a group of bands which form an arclike structure around $E = -0.8$ eV, which agrees well with the most intense features of the ARPES map. Concerning the Te p_z-projected bands, large intensity is seen for a flat band around the electron pocket, which has been identified as a surface state [14,15]. This corresponds to a bright flat line in the ARPES map at $k_x > 0.25$ Å^{-1}, $E \approx -0.1$ eV. By comparison with Figs. 3 and 4 it is clear that electron pocket and surface state can be best visualized with z-polarized light. This is in agreement with the experiments by Crepaldi *et al.* [15], who observed the surface state with strong intensity with mixed s- and p-polarized light (containing some z-polarization), while the surface state intensity almost vanished for pure s-polarized light (which contains zero z polarization). In z polarization, the electric field vector of the photon field is nearly parallel to the emission direction. This explains why the overall ARPES intensity is much larger than for in-plane (x or y) polarization. Experimentally, exact z polarization is impossible but can be approached by using p polarization and grazing incidence.

We note that Aryal and Manousakis [25] analyzed the ARPES polarization dependence of MoTe$_2$ by using the plane-wave approximation and assuming that the final state wave function does not depend on z. Thereby they obtained the same selection rules as we did for Te p initial states but somewhat different ones for Mo d initial states. For example, they predict that with y-polarized light there are no transitions from Mo d_{yz} initial states. However, the comparison between Figs. 4(a) and 4(c) strongly indicates that such transitions have a large oscillator strength along the $\bar{\Gamma}$-$\bar{X}$ line.

The foregoing analysis shows that the ARPES polarization dependence can qualitatively be understood from the orbital-projected DFT bands and the dipole selection rules. It is clear however, that such an initial state theory cannot give a quantitative description of ARPES intensity maps. Indeed, final state effects play an important role too and are responsible for the photon energy dependence. Note that the present one-step-model calculations include all matrix and final state effects.

Despite its qualitative nature, the analysis based on orbital-projected bands and selection rules is very useful for determining what polarization is best suited for probing particular parts of the band structure and for understanding the nature of the bonding. In the case of MoTe$_2$, we have seen that the electron pocket and the surface state can be observed with z polarization, whereby the Te p_z contribution is highlighted. x polarization reveals the Te p_x bands and is a good choice for observing the hole pocket. With y polarization, mainly Mo d_{xy} and d_{yz} orbitals are probed and form a group of linear dispersing bands which join either the electron or the hole pocket.

We also computed the ARPES intensity maps in the whole 2D Brillouin zone at the Fermi energy (see Fig. S4 in the Supplemental Material [38]). Concerning the polarization dependence, the same conclusion is reached as in the band structure analysis above, namely, that the electron and hole pockets are best observed with z and x polarized light, respectively. The spin-orbit coupling in MoTe$_2$ gives rise to a spin splitting of bands of the order of 0.5 eV [15]. Our one-step model calculations (Fig. S5 in the Supplemental Material [38]) show that this brings about a substantial spin polarization of the photoelectrons, which is especially pronounced at the surface state (see Fig. 2) when z-polarized light is used.

C. Comparison with experiment

Tamai *et al.* [17] measured the MoTe$_2$ ARPES along k_x with 60-eV light and p polarization, corresponding to a combination of x- and z-polarized light. Both electron and hole pockets were observed with high intensity. In contrast, s polarization suppresses the electron pocket and the surface state intensity as observed by Crepaldi *et al.* [15]. Both experimental results can be explained by our polarization analysis.

Here we have measured the ARPES of MoTe$_2$ near the Fermi energy along the $\bar{\Gamma}$-$\bar{X}$ line ($k_x < 0.4$ Å^{-1}) using a photon energy of 6.27 eV and s-polarized light (polarization vector along the y axis). See Fig. 1(c) for the experimental geometry. The experimental data are shown in Fig. 6, along with the corresponding one-step ARPES calculation. Here, the raw ARPES intensity is shown. The second derivative of the intensity with respect to the energy is often used to enhance the dispersion of broad spectra features. The corresponding experimental data are shown in Fig. S6 of the Supplemental Material [38]. Both the measured and calculated ARPES maps are dominated by a group of strongly dispersing bands, marked 2–4 in Fig. 6(a). As seen from the comparison with the projected bands [Figs. 6(c)–6(e)], these features are mainly of Mo d_{xy} and Mo d_{yz} character. Feature 4 may be assigned to the hole pocket, while features 1–3 belong to lower energy bands with similar dispersion. Features 5 and 6 are part of the electron pocket, where the intense band, 5, is dominated by Mo d_{xy} and d_{yz} orbitals, while the weak feature, 6, is essentially of Mo d_{yz} character. Experiment and theory disagree somewhat about the k_x positions of the various features. The calculated feature, 2, is shifted by 0.1 Å^{-1} to higher k_x with respect to experiment, which could be due to limitations of the surface barrier model used in the KKR calculations. Furthermore, the splitting between hole and electron pockets is smaller in the calculation than in experiment (features 4 and 5). Apart from these details, the calculated ARPES intensity map agrees very well with the data.

The ARPES calculations in Figs. 4(a) and 6(b) were obtained with the same light polarization but different photon energies, 60 and 6.27 eV, respectively. When comparing the same binding energy range, we find that the two ARPES intensity maps are very similar, except that with 6.27-eV photons, the average intensity is over one order of magnitude larger than with 60-eV photons.

D. Photon energy and k_z dependence

We have computed the ARPES from the Fermi level along the $\bar{\Gamma}$-$\bar{X}$ line as a function of photon energy in the energy range 50–160 eV. In the spirit of the three-step
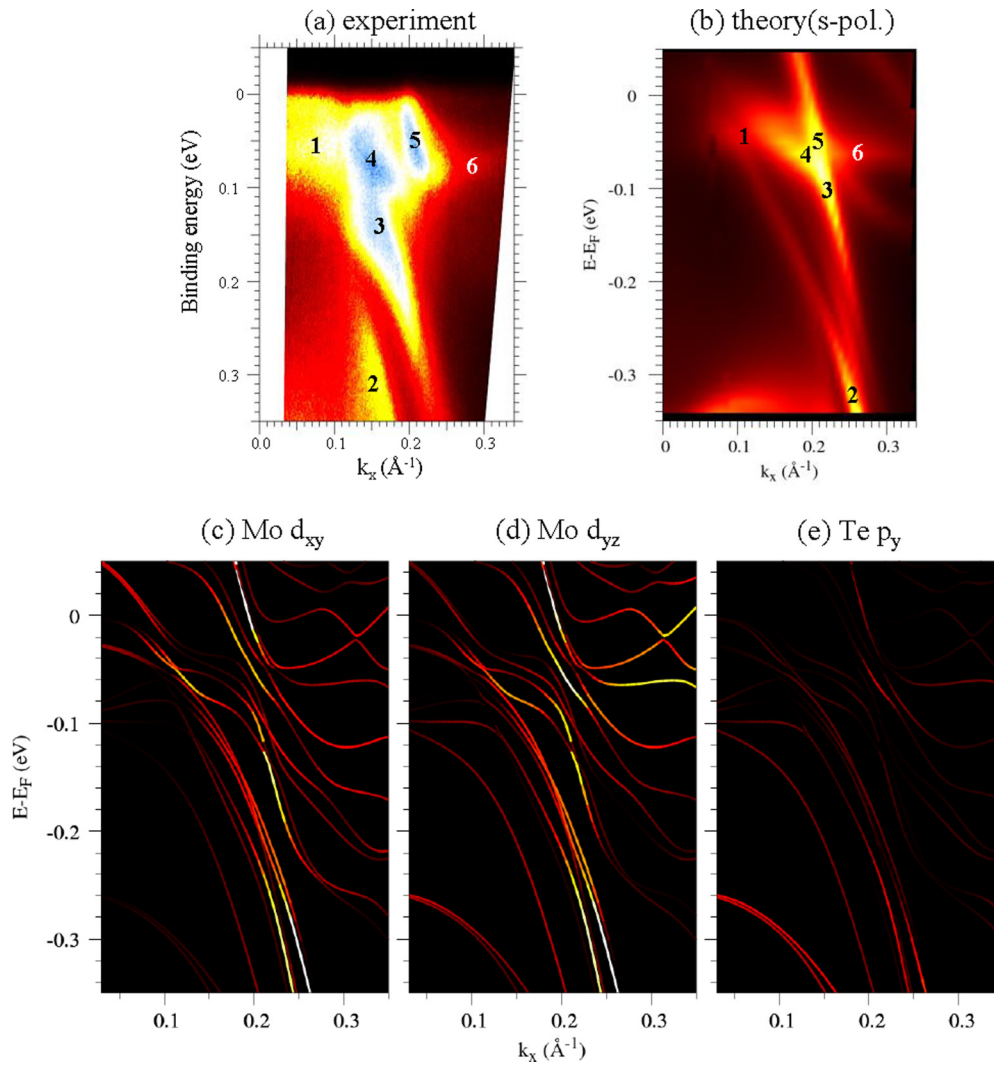
FIG. 6. Comparison between (a) experimental and (b) theoretical ARPES intensity maps for $\hbar\omega = 6.27$ eV and *s*-polarized light. (c)–(e) Corresponding orbital projected bands. These are the same data as in Fig. 4 plotted on an enlarged E scale for easy comparison with (a) and (b).
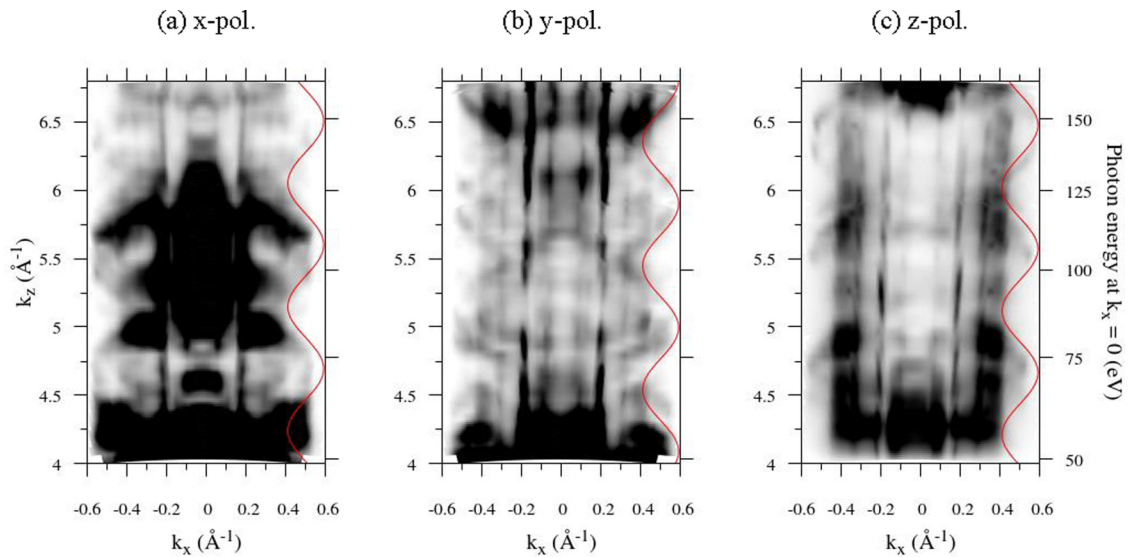

FIG. 7. k_x-k_z dispersion of the ARPES intensity calculated from the one-step model for (a) x polarization, (b) y polarization, and (c) z polarization. The red solid line is a cosine function with period $4\pi/c \approx 0.905$ Å^{-1}.

model, the photon energy has been converted to the final state photoelectron momentum k_z in the bulk by using $k_z = \sqrt{2m(E_{kin} + V_0)/\hbar^2 - k_{||}^2}$. Here E_{kin} is the kinetic energy of photoelectrons, and $V_0 = 16$ eV is the inner potential. The value of V_0 has been estimated from the work function $\phi = 4.1$ eV and the KKR interstitial potential and is comparable with that in Ref. [17]. The ARPES map intensity (Fig. 7) shows a strong dependence on k_z. The most intense bands have no k_z dispersion, indicating surface band character. However, the region 0.4 Å^{-1} < $|k_x|$ < 0.6 Å^{-1} especially displays a clear period of $4\pi/c \approx 0.905$ Å^{-1}. The $4\pi/c$ periodicity is in agreement with the data of Ref. [17] and was also observed in WTe$_2$ [41]. Our one-step calculations thus prove theoretically that some of the k_z dispersion of the MoTe$_2$ bulk band structure survives in the photoemission process and can be observed in ARPES. Interestingly, the period of the k_z oscillation is $4\pi/c$ rather than $2\pi/c$, the value expected from the band structure. The reason is that MoTe$_2$ has a nonsymmorphic space group with glide planes along c. As shown by Pescia *et al.* [42], for such space groups, final states change parity with respect to the glide plane when going from k_z to $k_z + 2\pi/c$. As a consequence photoemission transition is possible only for either of the two parity-related initial state bands. This effect has been observed in other layered materials, including graphite [42,43] and MoTe$_2$ (2H) [44].

IV. CONCLUSIONS

In summary, we have presented a combined experimental and theoretical study of the band structure of the Weyl semimetal candidate material MoTe$_2$(T_d). The orbital character of the near-Fermi-energy bands has been analyzed using density functional theory. We found that along the $\bar{\Gamma}$-$\bar{X}$ line, the hole pocket is dominated by the Te p_x orbital, while the electron pocket is mainly made of Mo d_{yz}- and Te p_z-derived bands. We have performed one-step-model ARPES calculations and obtained good agreement with the experimental data. The ARPES intensity depends strongly on the light polarization, which can be understood from the orbital character of the bands together with the dipole selection rules. The results show how relevant parts of the near-Fermi-energy band structure, especially electron pockets, hole pockets, and surface states, can be highlighted using the most suitable light polarization. The calculated ARPES maps have a complex photon energy dependence and display an approximate $4\pi/c$ periodicity in k_z, in agreement with experiment. More generally, we conclude that one-step-model ARPES calculations are indispensable for a quantitative interpretation of ARPES data with complex band structures typical for topological 2D materials.

[1] S. Y. Xu, I. Belopolski, N. Alidoust, M. Neupane, G. Bian, C. Zhang, R. Sankar, G. Chang, Z. Yuan, C. C. Lee, S. M. Huang, H. Zheng, J. Ma, D. S. Sanchez, B. K. Wang, A. Bansil, F. Chou, P. P. Shibayev, H. Lin, S. Jia, and M. Z. Hasan, Science **349**, 613 (2015).

[2] V. Aji, Phys. Rev. B **85**, 241101(R) (2012).

[3] A. A. Zyuzin and A. A. Burkov, Phys. Rev. B **86**, 115133 (2012).

[4] D. T. Son and B. Z. Spivak, Phys. Rev. B **88**, 104412 (2013).

[5] A. Burkov, Annu. Rev. Condens. Matter Phys. **9**, 359 (2018).

[6] H. B. Nielsen and M. Ninomiya, Phys. Lett. B **130**, 389 (1983).

[7] H. Weng, C. Fang, Z. Fang, B. A. Bernevig, and X. Dai, Phys. Rev. X **5**, 011029 (2015).

[8] B. Q. Lv, H. M. Weng, B. B. Fu, X. P. Wang, H. Miao, J. Ma, P. Richard, X. C. Huang, L. X. Zhao, G. F. Chen, Z. Fang, X. Dai, T. Qian, and H. Ding, Phys. Rev. X **5**, 031013 (2015).

[9] S.-M. Huang, S.-Y. Xu, I. Belopolski, C.-C. Lee, G. Chang, B. Wang, N. Alidoust, G. Bian, M. Neupane, C. Zhang, S. Jia, A. Bansil, H. Lin, and M. Z. Hasan, Nat. Commun. **6**, 7373 (2015).

[10] A. A. Soluyanov, D. Gresch, Z. Wang, Q. Wu, M. Troyer, X. Dai, and B. A. Bernevig, Nature (London) **527**, 495 (2015).

[11] Z. Wang, D. Gresch, A. A. Soluyanov, W. Xie, S. Kushwaha, X. Dai, M. Troyer, R. J. Cava, and B. A. Bernevig, Phys. Rev. Lett. **117**, 056805 (2016).

[12] T.-R. Chang, S.-Y. Xu, G. Chang, C.-C. Lee, S.-M. Huang, B. Wang, G. Bian, H. Zheng, D. S. Sanchez, I. Belopolski, N. Alidoust, M. Neupane, A. Bansil, H.-T. Jeng, H. Lin, and M. Z. Hasan, Nat. Commun. **7**, 10639 (2016).

[13] M. Fanciulli, J. Schusser, M.-I. Lee, Z. E. Youbi, O. Heckmann, M. C. Richter, C. Cacho, C. Spezzani, D. Bresteau, J.-F. Hergott, P. D'Oliveira, O. Tcherbakoff, T. Ruchon, J. Minár, and K. Hricovini, Phys. Rev. Res. **2**, 013261 (2020).

[14] Y. Sun, S.-C. Wu, M. N. Ali, C. Felser, and B. Yan, Phys. Rev. B **92**, 161107(R) (2015).

[15] A. Crepaldi, G. Autès, A. Sterzi, G. Manzoni, M. Zacchigna, F. Cilento, I. Vobornik, J. Fujii, P. Bugnon, A. Magrez, H. Berger, F. Parmigiani, O. V. Yazyev, and M. Grioni, Phys. Rev. B **95**, 041408(R) (2017).

[16] J. Jiang, Z. K. Liu, Y. Sun, H. F. Yang, C. R. Rajamathi, Y. P. Qi, L. X. Yang, C. Chen, H. Peng, C.-C. Hwang, S. Z. Sun, S.-K. Mo, I. Vobornik, J. Fujii, S. S. P. Parkin, C. Felser, B. H. Yan, and Y. L. Chen, Nat. Commun. **8**, 13973 (2017).

[17] A. Tamai, Q. S. Wu, I. Cucchi, F. Y. Bruno, S. Riccò, T. K. Kim, M. Hoesch, C. Barreteau, E. Giannini, C. Besnard, A. A. Soluyanov, and F. Baumberger, Phys. Rev. X **6**, 031021 (2016).

[18] B. E. Brown, Acta Cryst. **20**, 268 (1966).

[19] H. P. Hughes and R. H. Friend, J. Phys. C **11**, L103 (1978).

[20] T. Zandt, H. Dwelk, C. Janowitz, and R. Manzke, J. Alloys Compd. **442**, 216 (2007).

[21] Y. Qi, P. G. Naumov, M. N. Ali, C. R. Rajamathi, W. Schnelle, O. Barkalov, M. Hanfland, S.-C. Wu, C. Shekhar, Y. Sun, V. Süss, M. Schmidt, U. Schwarz, E. Pippel, P. Werner, R. Hillebrand, T. Förster, E. Kampert, S. Parkin, R. J. Cava, C. Felser, B. Yan, and S. A. Medvedev, Nat. Commun. **7**, 11038 (2016).

[22] A. P. Weber, P. Rüßmann, N. Xu, S. Muff, M. Fanciulli, A. Magrez, P. Bugnon, H. Berger, N. C. Plumb, M. Shi, S. Blügel, P. Mavropoulos, and J. H. Dil, Phys. Rev. Lett. **121**, 156401 (2018).

[23] P. Puschnig, S. Berkebile, A. J. Fleming, G. Koller, K. Emtsev, T. Seyller, J. D. Riley, C. Ambrosch-Draxl, F. P. Netzer, and M. G. Ramsey, Science **326**, 702 (2009).

[24] C. Datzer, A. Zumbülte, J. Braun, T. Förster, A. B. Schmidt, J. Mi, B. Iversen, P. Hofmann, J. Minár, H. Ebert, P. Krüger, M. Rohlfing, and M. Donath, Phys. Rev. B **95**, 115401 (2017).

[25] N. Aryal and E. Manousakis, Phys. Rev. B **99**, 035123 (2019).

[26] A. M. Bradshaw and D. P. Woodruff, New J. Phys. **17**, 013033 (2015).

[27] G. Kresse and J. Furthmüller, Phys. Rev. B **54**, 11169 (1996).

[28] J. P. Perdew, K. Burke, and M. Ernzerhof, Phys. Rev. Lett. **77**, 3865 (1996).

[29] H. Ebert, D. Ködderitzsch, and J. Minár, Rep. Prog. Phys. **74**, 096501 (2011).

[30] J. Braun, H. Ebert, and J. Minár, in *Spintronics: From Materials to Devices*, edited by C. Felser and G. H. Fecher (Springer, Dordrecht, 2013), pp. 97–114.

[31] J. Minár, J. Braun, S. Mankovsky, and H. Ebert, J. Electron Spectrosc. Relat. Phenom. **184**, 91 (2011).

[32] J. Braun, J. Minár, and H. Ebert, Phys. Rep. **740**, 1 (2018).

[33] J. Braun, Rep. Prog. Phys. **59**, 1267 (1996).

[34] F. Máca and M. Scheffler, Comput. Phys. Commun. **51**, 381 (1988).

[35] K. Kambe, in *Computational Methods in Band Theory: Proceedings of a Conference Held at the IBM Thomas J. Watson Research Center, Yorktown Heights, New York, 1970, under the Joint Sponsorship of IBM and the American Physical Society*, edited by P. M. Marcus, J. F. Janak, and A. R. Williams (Springer, Boston, 1971), pp. 409–415.

[36] J. Schusser, L. Nicolaï, M. Fanciulli, M.-i Lee, Z. E. Youbi, O. Heckmann, C. Richter, K. Hricovini, and J. Minár, AIP Conf. Proc. **2131**, 20041 (2019).

[37] H. Iwasawa, E. F. Schwier, M. Arita, A. Ino, H. Namatame, M. Taniguchi, Y. Aiura, and K. Shimada, Ultramicroscopy **182**, 85 (2017).

[38] See Supplemental Material at http://link.aps.org/supplemental/10.1103/PhysRevB.103.125139 for further details: (i) the density of states, (ii) projected bands for all orbitals, (iii) ARPES intensity at Fermi energy, (iv) spin-polarized ARPES, and (v) a second derivative plot of experimental ARPES data.

[39] S. Goldberg, C. Fadley, and S. Kono, J. Electron Spectrosc. Relat. Phenom. **21**, 285 (1981).

[40] P. Krüger, J. Phys. Soc. Jpn. **87**, 061007 (2018).

[41] D. Di Sante, P. K. Das, C. Bigi, Z. Ergönenc, N. Gürtler, J. A. Krieger, T. Schmitt, M. N. Ali, G. Rossi, R. Thomale, C. Franchini, S. Picozzi, J. Fujii, V. N. Strocov, G. Sangiovanni, I. Vobornik, R. J. Cava, and G. Panaccione, Phys. Rev. Lett. **119**, 026403 (2017).

[42] D. Pescia, A. Law, M. Johnson, and H. Hughes, Solid State Commun. **56**, 809 (1985).

[43] F. Matsui, H. Nishikawa, H. Daimon, M. Muntwiler, M. Takizawa, H. Namba, and T. Greber, Phys. Rev. B **97**, 045430 (2018).

[44] T. Böker, R. Severin, A. Müller, C. Janowitz, R. Manzke, D. Voß, P. Krüger, A. Mazur, and J. Pollmann, Phys. Rev. B **64**, 235305 (2001).